ISSN 0031-918X, The Physics of Metals and Metallography, 2015, Vol. 116, No. 11, pp. 1165–1174. © Pleiades Publishing, Ltd., 2015.
Original Russian Text © V.A. Dudko, A.E. Fedoseeva, A.N. Belyakov, R.O. Kaibyshev, 2015, published in Fizika Metallov i Metallovedenie, 2015, Vol. 116, No. 11, pp. 1222–1232.

STRENGTH AND PLASTICITY

Influence of the Carbon Content on the Phase Composition and Mechanical Properties of P92-Type Steel

V. A. Dudko, A. E. Fedoseeva, A. N. Belyakov, and R. O. Kaibyshev

Belgorod State University, ul. Pobedy 85, Belgorod, 308034 Russia

e-mail: dudko@bsu.edu.ru

Received April 22, 2015; in final form May 15, 2015

Abstract—The deformation behavior and the microstructure evolution under the creep of 10Kh9V2MFBR steel (Russian analog of the P92 steel) (in wt %, Fe–8.9% Cr–0.05% Si–0.2% Mn–1.9% W–0.5% Mo–0.25% V–0.07Nb–0.08% N–0.01% B) with the standard (0.1%) and lowered (0.018%) carbon contents have been investigated. After the heat treatment, which included normalizing at 1050°C and tempering at 720–750°C, carbides $M_{23}C_6$ and carbonitrides M(C,N) are formed in the 10Kh9V2MFBR steel, while in the 02Kh9V2MFBR steel (modified P92 steel), carbides $M_{23}C_6$, nitrides M_2N, and carbonitrides M(C,N) as well as δ-ferrite (23%) were found. The measurements of hardness and tensile tests at room and elevated temperatures did not reveal substantial distinctions in the short-term mechanical properties of both steels. The hardness of steels after tempering was 220 *HB*. At the same time, the creep characteristics of the steels were found to be different. A decrease in the carbon content leads to an increase in the long-term creep strength and creep limit at 650°C for short-term tests with time-to-fracture shorter than 10^3 h. The time to fracture of steels with various carbon contents is almost the same in long-term creep tests. Factor responsible for such effect of carbon on the creep strength are discussed.

Keywords: creep, heat-resistant martensitic steels, long-term creep strength, carbides

DOI: 10.1134/S0031918X15110058

INTRODUCTION

Currently, the high-chromium martensitic steels are widely used to fabricate the elements of power plants operating at a steam temperature above 570°C, since these steels possess high heat resistance [1, 2]. The high creep resistance of these steels is caused by the stability of their microstructure, which represents tempered martensite lath structure (TMLS), under the conditions of high temperatures and applied stresses [1–3]. This stability is provided by two types of particles of second phases that precipitate during tempering, as well as by the Laves phase, which is precipitated during short-term aging and creep [1, 2, 4–9]. The particles of the carbides $M_{23}C_6$ and of the Laves phase Fe_2(W,Mo) have dimensions larger than 100 nm and are located at low-angle and high-angle boundaries (HABs) [4, 5]. They can coalesce both during creep and during the long-term aging [4–6]. The carbonitrides M(C,N) are located uniformly in the bulk of grains and are stable to coalescence due to the two-phase separation into V- and N-enriched and Nb- and C-enriched particles [1, 2, 4, 5, 7–11]. The first ones have the form of winglets (platelets) up to 10 nm in length and up to 4 nm thick, while the second ones are round and have sizes of 30–50 nm [4, 5, 10–12].

Up to now, the mechanism that provides the unique creep resistance of steels with 9–11 wt % Cr remains unclear [1, 4–6]. It was long believed [1, 3, 9] before the appearance of publications [4–6] that the high heat resistance of high-chromium steels of the last generation is caused by the suppression of the migration of boundaries in the TMLS due to high retarding Zener force [13] associated with M(C,N) carbonitrides. The authors of [12, 14, 15] proposed an original approach to the alloying of the 9%Cr steels, which made it possible to increase the time-to-fracture by a factor of almost 100. Since nitrogen cannot be substituted for carbon in the $M_{23}C_6$ carbides, a decrease in the carbon content substantially decreases the volume fraction of these carbides. Simultaneously, the volume fraction of the carbonitrides M(C,N) increases, the stability of which against the coalescence is substantially higher than that of the for $M_{23}C_6$ carbides [16, 17]. This circumstance increases the structural stability of the TMLS upon creep and, correspondingly, the long-term creep strength of high-chromium martensitic steels [6, 12, 14, 15, 18–20]. At the same time, it is hardly possible to draw the conclusion that an increase in the heat resistance of these steels is due to the lowering of the carbon content based on the results of the above-mentioned studies, since, simultaneously with a decrease in the carbon content in these steels, the Co content was increased in them in order to retain invariable the content of austenite-forming ele-

ments, which is expressed as the nickel equivalent (wt %) as follows [21]:

$$Ni_{eq} = Ni + Co + 0.5Mn + 0.3Cu + 25N + 30C.$$

According to this equivalent, to compensate for a decrease in the carbon content from 0.1 to 0.02 wt %, it is required to introduce approximately 3 wt % Co [1, 12, 14, 15], which substantially decreases the rate of diffusion processes [22]. The need to hold the magnitude of Ni_{eq} invariable is caused by an inadmissibility of the formation of δ ferrite, which, according to the modern concepts, decreases the creep resistance of steels. It was established for 12%Cr steels, which contain 0.1 wt % C, the worsening of the properties is caused by the appearance of a phase in the material, the creep limit of which is lower than that of TMLS [1, 23, 24].

The experimental data that could confirm the validity of this regularity for 9%Cr steels with a low carbon content are absent in the literature. This study is aimed at a detailed consideration of the influence of lowering of the carbon content, which was partially compensated by an increase in the nitrogen content, on the phase composition and mechanical properties of the P92-type steel with 9%Cr. This steel possesses the highest heat resistance among the new-generation cobalt-free commercial steels [1]. This investigation is performed in the scope of a complex study, which is targeted to the reveal of the role of carbonitrides *M*(C,N) in the heat resistance of high-chromium martensitic steels, which should make it possible to develop approaches to an increase in their long-term creep strength due to the variation in the type of alloying and heat treatment.

EXPERIMENTAL

We investigated two steels: a standard 10Kh9V2MFBR steel of composition Fe–0.1C–8.75Cr–0.17Si–0.54Mn–1.60W–0.51Mo–0.23V–0.07Nb–0.04N–0.003B–0.21Ni; and the 02Kh9V2MFBR (modified P92) steel with a lowered carbon content and elevated nitrogen content, of composition Fe–0.018C–8.9Cr–0.05Si–0.2Mn–1.9W–0.5Mo–0.25V–0.07Nb–0.08N–0.01B (in wt %). Both steels were normalized at 1050°C and then tempered at 720–750°C for 3 h. The tensile tests were performed at 20, 450, 550, and 650°C. Flat samples with a cross section of ~7 × 3 mm and a length of the gage part of 25 mm were cut out from the ingots of the 10Kh9V2MFBR and 02Kh9V2MFBR steels and tested for creep at 650°C with initial applied stresses of 118, 140, 160, 180, and 200 MPa.

The structural investigations of the samples were performed using a Quanta 600FEG scanning electron microscope equipped with an attachment for electron backscatter diffraction (EBSD) with an automated system to analyze the orientations. The foils for the transmission electron microscopy (TEM) were prepared by jet electropolishing in a 10% solution of perchloric acid in acetic acid. To analyze the chemical composition and the nature of particles of second phases, we used the method of carbon replicas. Thin foils and carbon replicas with extracted particles of second phases were investigated using a JEOL JEM-2100 transmission electron microscope at an accelerating voltage of 200 kV, which was equipped with an INCA attachment for energy dispersive analysis of the chemical composition of the particles. The sizes of laths/subgrains were measured by the intercept method using TEM micrographs. The dislocation density was determined by counting dislocations inside grains/subgrains using six arbitrarily selected electron-microscopy images for each point. The details of structural investigations were presented in [4–6, 11, 22].

The volume fraction of the particles of the second phases was calculated with the help of the ThermoCalc program using the TCFE6 database.

The Vickers microhardness was measured at a load of 0.1 N after normalizing of the steels. The volume fraction of δ ferrite was determined from the data on the microhardness distribution over the sample surface [25]. The Brinell hardness of both steels was determined after tempering.

RESULTS

Microstructure after Normalizing and Tempering

The characteristics of the microstructure of both steels after tempering and creep tests to failure under a stress of 118 MPa are presented in Table 1. The characteristic maps of misorientations of the structural elements in steels after tempering are shown in Fig. 1. Packet martensite is formed in both steels upon normalizing, which is quenching for this material from the viewpoint of the theory of heat treatment. The structure of the packet martensite is analyzed according to the scheme presented in [26]. The average size of the prior austenite grains was 20 μm for the 10Kh9V2MFBR steel (Fig. 1a) and 15 μm for the modified 02Kh9V2MFBR steel (Fig. 1b). An important distinction of the structures of these two steels is the presence of grains of δ ferrite, which in the 02Kh9V2MFBR steel are observed in the form of separate grains, in which any substructure is absent (Fig. 1b). After normalizing, the microhardness of the δ-ferrite grains (318 ± 10 *HV*) differs substantially from the microhardness of martensite (483 ± 14 *HV*), which allowed us to determine, with a high accuracy, its volume fraction, which constituted 23%. Since the δ ferrite contains no packets/blocks, its appearance determines the larger distance between HABs in the 02Kh9V2MFBR steel.

The dislocation structure of the lath martensite is retained in steel after tempering. A decrease in the carbon content leads to a decrease in the transverse dimension of laths from 0.33 to 0.29 μm (Fig. 2, Table 1); the dislocation density lowers more than twofold.

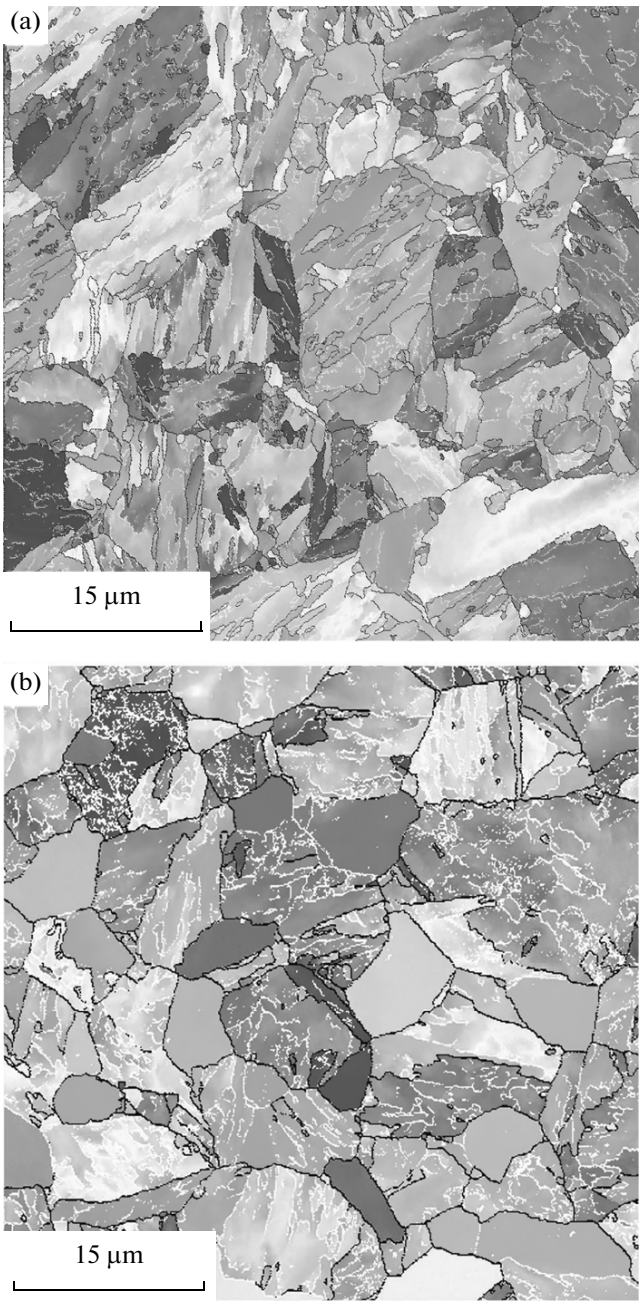

Fig. 1. Misorientation maps of structural elements in steels (a) 10Kh9V2MFBR and (b) 02Kh9V2MFBR after tempering.

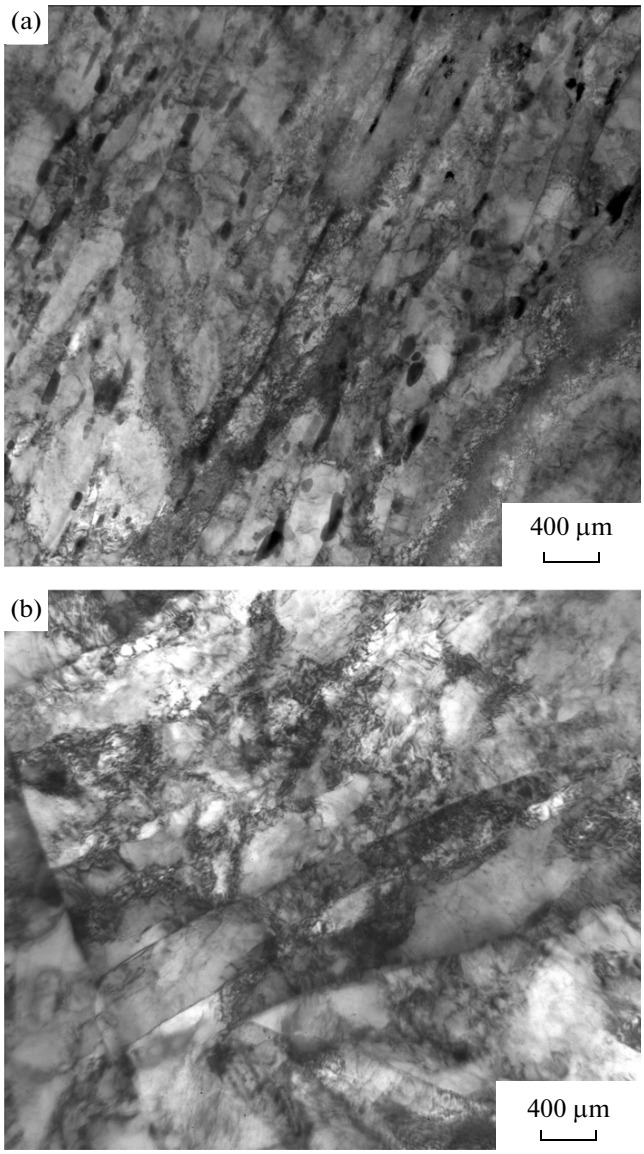

Fig. 2. Tempered martensite lath structure of (a) the 10Kh9V2MFBR steel and (b) low-carbon 02Kh9V2MFBR steel after tempering.

It should be noted that in an analogous low-carbon steel with an addition of 3 wt % Co, which was studied in [18], the thickness of martensite laths after tempering is less (240 μm) and the density of dislocations is somewhat larger ($\rho \sim (4.0 \pm 0.9) \times 10^{14}$ m^{-2}) than in the steel without cobalt that is studied in this work. This is explained by the fact that the dislocation density in δ-ferrite grains in the 02Kh9V2MFBR steel is lower approximately by a factor of 7–10 as compared to martensite crystals.

The structures of the two steels differ most strongly in the phase composition. Figure 3 shows typical particles of the second phases in the 10Kh9V2MFBR steel. The tempering at 720°C leads to the formation of $M_{23}C_6$ carbides (Fig. 3) with an average size of 110 nm. The carbonitrides M(C,N) are divided by the chemical composition into vanadium-enriched or niobium-enriched (Fig. 3b). The V(C,N) carbonitrides have a characteristic shape of "winglets," while the Nb(C,N) particles are round. The average size of carbonitrides after tempering in the 10Kh9V2MFBR steel was 31 nm. The examination of carbon replicas of the 02Kh9V2MFBR steel in TEM showed the presence of carbonitrides M(C,N), nitrides $(Cr,V)_2N$, and carbides $M_{23}C_6$. A decrease in the carbon content and

Table 1. Microstructural parameters of steels after tempering and creep at 650°C and 118 MPa

	Tempering		Creep	
	10Kh9V2MFBR	02Kh9V2MFBR	10Kh9V2MFBR	02Kh9V2MFBR
Average thickness of subgrains/laths, μm	0.33 ± 0.05	0.29 ± 0.05	0.74 ± 0.05	0.79 ± 0.05
Dislocation density inside the laths, m^{-2}	$(6.2 \pm 0.7) \times 10^{14}$	$(2.7 \pm 0.3) \times 10^{14}$	$(1.0 \pm 0.4) \times 10^{14}$	$(3.4 \pm 0.6) \times 10^{13}$
Average size $M_{23}C_6$, nm	110 ± 20	~500	195 ± 39	~500
Volume fraction $M_{23}C_6$, %	1.79	0.5	1.79	0.3
Average size M_2N, nm	–	72 ± 20	–	108 ± 21
Volume fraction M_2N, %	–	0.07	–	0.07
Average size M(C,N), nm	31 ± 15	15 ± 5	46 ± 24	37 ± 20
Volume fraction M(C,N), %	0.23	0.45	0.23	0.45
Average size Fe_2W, nm	–	–	303 ± 47	330 ± 50
Volume fraction Fe_2W, %	–	–	1.17	2.0
Volume fraction of δ ferrite, %	0	23	0	23
Distance between HAB, μm	2.6 ± 0.4	6.0 ± 1.0	4.5 ± 0.8	5.8 ± 1.0

Table 2. Mechanical properties of the standard and modified steels

Test temperature, °C	10Kh9V2MFBR			02Kh9V2MFBR		
	Offset yield stress, MPa	Ultimate strength, MPa	Relative elongation, %	Offset yield stress, MPa	Ultimate strength, MPa	Relative elongation, %
20	490	700	18.0	620	710	12.8
450	405	525	13.5	415	560	8.9
550	385	430	14.5	345	475	15.9
650	260	285	23.5	235	250	16.5

an increase in the nitrogen content led to the formation of elongated particles of $(Cr,V)_2N$ nitrides with an average size of 72 nm in this steel (Fig. 4a). In the modified steel, complex carbonitrides M(C,N) with an average size of 15 nm are precipitated. This means that a decrease in the carbon content suppressed the two-phase separation of the carbonitrides into V-enriched or Nb-enriched particles. All of them contain the same amounts of vanadium and niobium (Fig. 4b). The carbonitrides M(C,N) and nitrides $(Cr,V)_2N$ are uniformly distributed over the matrix volume; their distribution in 02Kh9V2MFBR steel is identical both inside the martensite crystals and inside the δ-ferrite grains. In the replicas of the steel with a low carbon content, few coarse (~500 nm in size) particles of $M_{23}C_6$ were found (Fig. 4).

Mechanical Properties of Steels after Normalizing and Tempering

Despite the distinctions in the structure, nature, volume fractions, and distribution of second-phases particles in the steels with different carbon contents, their hardness differs insignificantly. The Brinell hardness of both steels after tempering was 220*HB*. No valuable distinctions in the mechanical behavior after tension at room and elevated temperatures were observed (Table 2).

In the low-carbon steel, the minimum creep rate $\dot{\varepsilon}_{min}$ is lower by a factor of approximately two to three at all applied stresses than that in the standard P92 steel (Figs. 5a, 5b). A decrease in $\dot{\varepsilon}_{min}$ leads to an increase in the time-to-fracture almost by a factor of 1.5–2 (Fig. 5c). When lowering the applied stress in the 10Kh9V2MFBR steel from 200 to 100 MPa, the initial creep rate decreases no more than by a factor of ten, whereas the minimum creep rate decreases by a factor of 1000 (Fig. 5a). Consequently, a decrease in applied stresses in the 10Kh9V2MFBR steel mainly leads to a decrease in the minimum creep rate. At all applied stresses, the minimum creep rate is attained after the strain becomes more than 1%. At strains of 1–4%, the creep rate remains almost unchanged and, at $\varepsilon > 4\%$, the accelerated creep stage begins. In the 02Kh9V2MFBR steel, a decrease in the applied stresses leads to a decrease in both $\dot{\varepsilon}_{min}$ and the creep strain, after which the stage of accelerated fracture

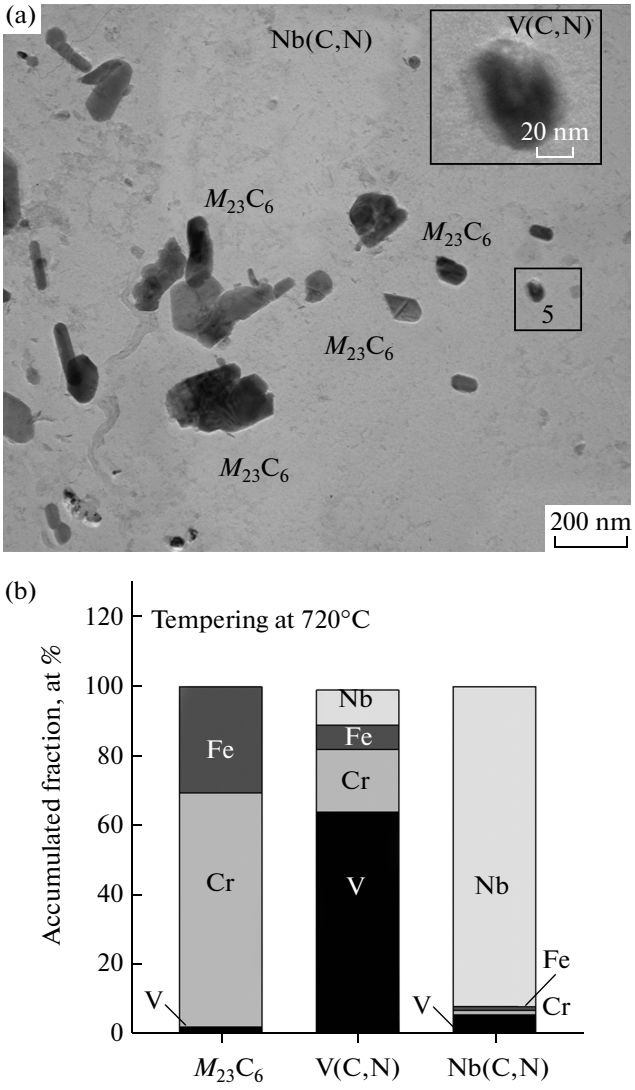

Fig. 3. (a) Typical particles of second phases in carbon replica and (b) their average chemical composition in the 10Kh9V2MFBR steel after tempering at 720°C.

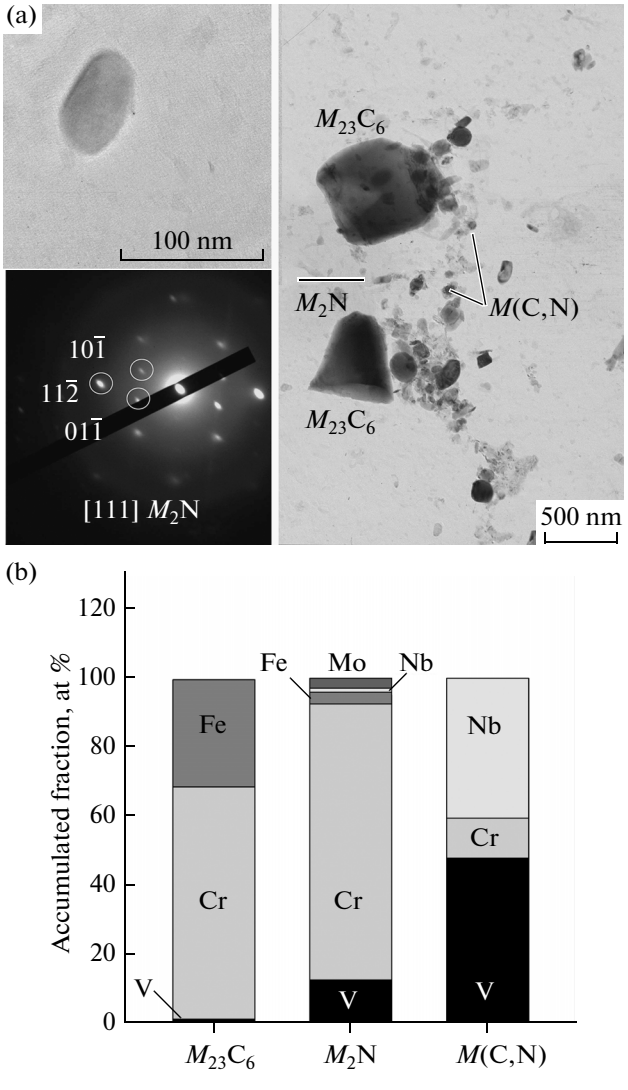

Fig. 4. (a) Typical particles of second phases in carbon replica and (b) their average chemical composition in the low-carbon 02Kh9V2MFBR steel after tempering at 750°C.

comes (Fig. 5b). The authors of [6] found a similar behavior of low-carbon steel with 3 wt % Co under creep; however, unlike the 02Kh9V2MFBR steel, a decrease in the applied stresses led to a decrease in the initial creep rate.

In the low-carbon steel without Co, the stage of steady-state flow at applied stress of 200 MPa starts almost immediately after the creep onset; at lower applied stresses, a clearly pronounced stage of transient creep appears. The extension of the stage of steady-state creep shortens compared to the P92 steel with a normal carbon content. At 118 MPa, the carbon content does not affect the shape of the dependence of the strain rate on the strain (Figs. 5a, 5b). The creep starts from an extended transient stage, in which the strain rate decreases by two orders of magnitude for the 10Kh9V2MFBR steel and by three orders of magnitude for the 02Kh9V2MFBR steel. At the beginning of the tests, the creep rate is the same for both materials (10^{-6} s^{-1}). It is ten times lower than that at an applied stress of 200 MPa.

The carbon content affects the dependence of the time-to-fracture on the applied stresses (Fig. 5c). However, it should be noted that the experimental result found in this study for the 10Kh9V2MFBR steel correlates with the published data for the P92 steel [27]. In the 02Kh9V2MFBR steel, the point of the bend in the dependence , which characterizes the change in the rate $d(\log\sigma)/d(\log\tau)$, is shifted toward shorter times to fracture (Fig. 5c). This point is usually observed in long-term tests ($\tau > 10000$ h) [1, 9, 28–30]. This means that a decrease in the carbon content substantially accelerates the creep in the long-term tests, which is the main disadvantage of P92-type steels.

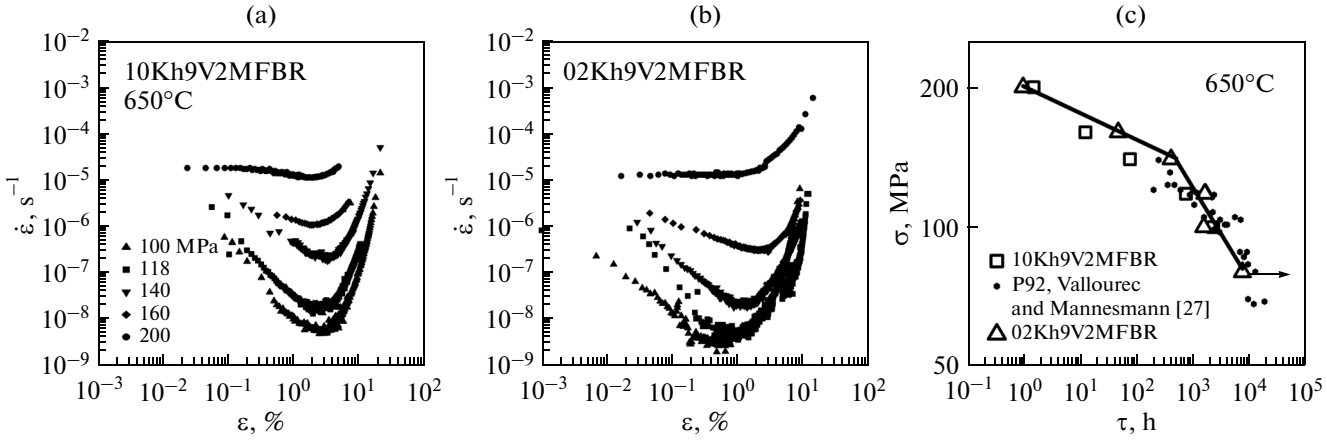

Fig. 5. (a, b) Dependences of the creep rates on the deformation strain and (c) dependence of applied stress on the time-to-fracture for steels 10Kh9V2MFBR and 02Kh9V2MFBR. The arrow near the point means that the tests were not finished.

Correspondingly, the long-term creep strength of steel with a low carbon content during the short-term tests (up to 2×10^3 h) is higher than for steel with 0.1 wt % C. However, in long-term tests, low-carbon steel does not show greater long-term strength.

Microstructure after Creep Tests

The results of the quantitative analysis of the microstructure after creep tests to fracture at 650°C and 118 MPa are presented in Table 1, the misorientation maps are presented in Fig. 6, and the fine structure is shown in Fig. 7. An analysis of the particles of second phases is presented in Figs. 8 and 9. It is known [5] that, in P92 steel, long-term aging at 650°C hardly affects the dislocation structure of the TMLS. The dislocation structure of the martensite is retained in the 10Kh9V2MFBR steel upon creep, even after the onset of the stage of accelerated creep [5]. In this case, the dislocations are rearranged into lath boundaries, which leads to the transformation of these boundaries into subgrain boundaries that exhibit small long-range fields of elastic stresses [5].

After the fracture, the microstructure consists of grains, some of which are elongated (which indicates that they form from martensite packets) [5, 26], while others are equiaxed (Fig. 6a). In these grains, the bulging of separate segments of HABs is observed, which is characteristic of hot-deformed structures [31]. The TEM study (Fig. 7a) revealed regions with laths, the width of which increased almost by a factor of 2.5 compared to the initial measurement (Table 1). These regions alternate with the regions of equiaxed subgrains with a size equal to the lath width. The dislocation density lowered sixfold (Table 1). At the stage of accelerated fracture, the transformation of the dislocation structure of packet martensite [31] into a polygonized structure started [5]. This is accompanied by the growth of the grain, since the distance between the HABs increases by 73% (Table 1).

The grains in the 02Kh9V2MFBR steel become equiaxed after the creep tests (Fig. 6b). In this case, no HAB migration occurs, since the distance between them remains invariable (Table 1). At the same time, the lath structure of the packet martensite is transformed into a subgrain structure (Fig. 7b), and the subgrain size in the steel with a low carbon content is equal to the subgrain size in the 10Kh9V2MFBR steel. The polygonization in the 02Kh9V2MFBR steel leads to a more than eightfold decrease in the dislocation density (Table 1). This is absolutely untypical of low-carbon steels containing 3 wt % Co, in which the dislocation density decreases by just threefold and in the neck zone only, whereas in the gage part, where no deformation localization occurs, the dislocation density is independent of the creep strain [18]. It should be noted that the δ-ferrite grains and the former regions of packet martensite are structurally indistinguishable after the fracture.

A decrease in the carbon content led to an almost twofold increase in the amount of the Laves phase precipitated during the creep (Table 1). In both steels, this phase precipitates preferentially along HABs (Fig. 7). The size of $Fe_2(W,Mo)$ particles in both steels is approximately the same. A specific feature of the 02Kh9V2MFBR steel is a high W/Mo ratio in the particles of the Laves phase, which equals three. The W/Mo ratio in similar low-carbon steels described in [6, 14] varies from five to seven, which is two times larger that the ratio of these elements in the chemical composition of the steel. The W/Mo ratio in $Fe_2(W,Mo)$ particles in the 10Kh9V2MFBR steel coincides with their ratio in the chemical composition; i.e., a decrease in the carbon content not only leads to an almost twofold decrease in the equilibrium content of $\Sigma(W + Mo)$ in the solid solution, but also to the almost complete escape of W (which decreases the diffusion rate more efficiently than Mo and, correspondingly, suppresses the recovery and polygoniza-

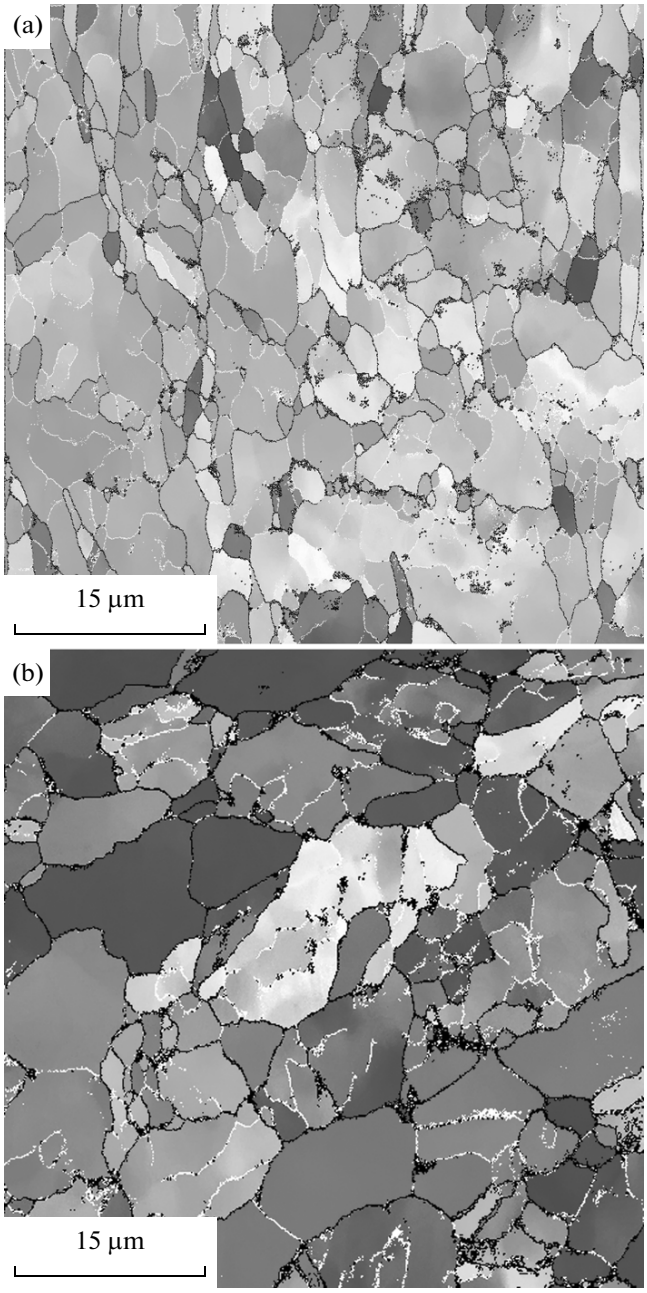

Fig. 6. Misorientation maps of structural elements in steels (a) 10Kh9V2MFBR and (b) 02Kh9V2MFBR after the creep tests at 650°C and 118 MPa.

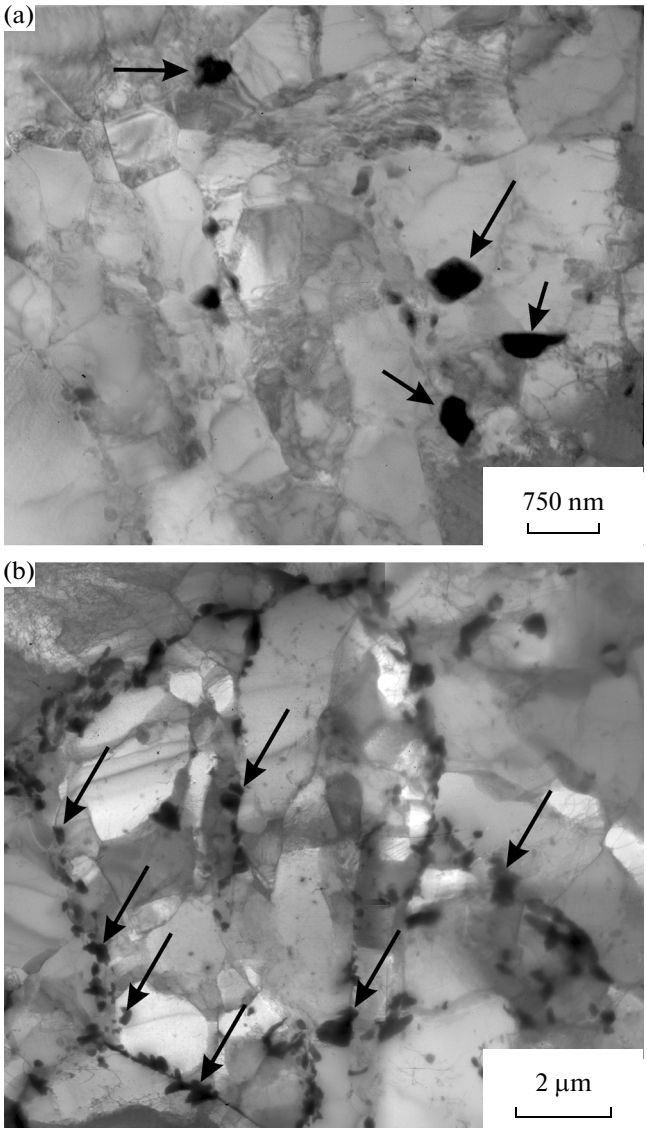

Fig. 7. Lath structure of (a) 10Kh9V2MFBR steel and (b) 02Kh9V2MFBR steel after the creep tests at 650°C and 118 MPa. Arrows show the characteristic particles of the Laves phase.

tion processes in high-chromium steels [1]) out of ferrite, while a significant part of Mo remains in it.

During creep in the 10Kh9V2MFBR steel, an increase occurs in the average size of $M_{23}C_6$ carbides from 110 to 195 nm (Fig. 8a, Table 1). Only round (M(C,N) carbonitride particles remain in the structure (Fig. 8a). In this case, the two-phase separation of carbonitrides into V-enriched or Nb-enriched is retained (Fig. 8b).

The size of carbides in the steel with a low carbon content remained invariable after creep, although some coarse particles of $M_{23}C_6$ carbides (about 500 nm in size) were found. They cannot introduce a noticeable contribution to the retardation of the migration of boundaries and dislocation motion. The average size of particles of M_2N nitrides increased upon creep from 72 to 108 nm (Fig. 9a), and the vanadium content in them decreased from 20 to 13 at %, while the chromium content increased from 70 to 80 at % (Fig. 9b). The creep at 650°C and 118 MPa does not lead to an essential change in the shape and distribution of nitrides. No two-phase separation of the M(C,N) carbonitrides, which takes place in the 10Kh9V2MFBR steel (Fig. 8b), appears after long-term aging and

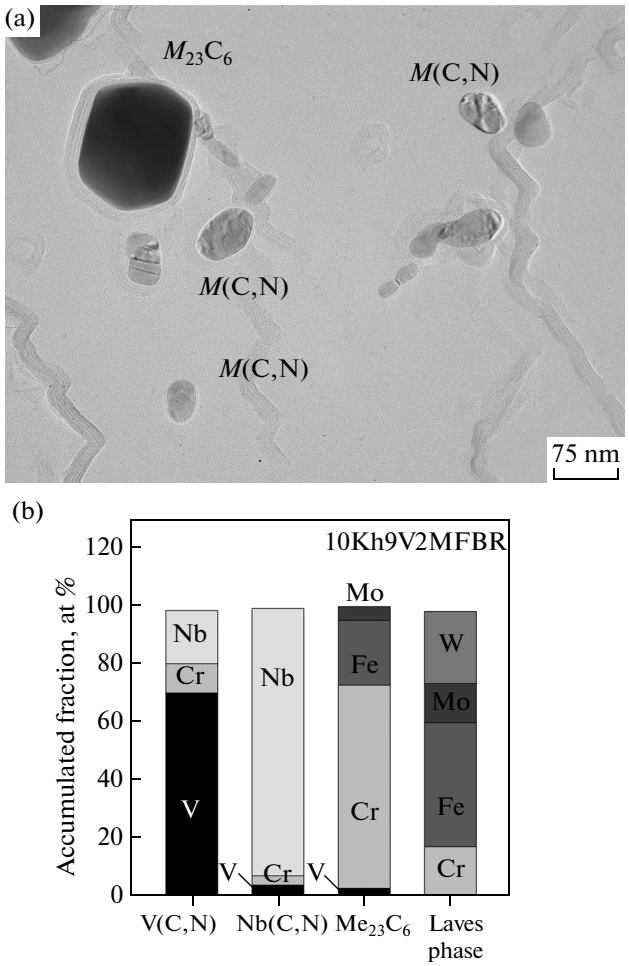

Fig. 8. (a) Typical particles of second phases in carbon replica and (b) their average chemical composition in the 10Kh9V2MFBR steel after the creep tests at 650°C for 118 MPa.

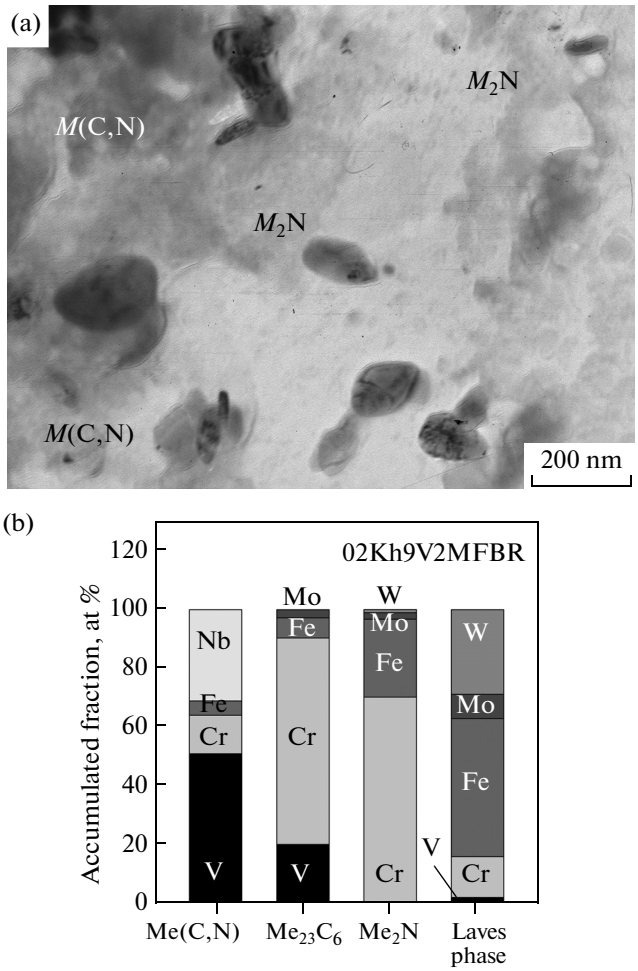

Fig. 9. (a) Typical particles of second phases in carbon replica and (b) their average chemical composition in the 02Kh9V2MFBR steel after the creep tests at 650°C for 118 MPa.

creep. The V/Nb ratio in most M(C,N) carbonitrides in the low-carbon steel is close to 1.6 (Fig. 9b), which is smaller than the ratio of these elements in the chemical composition of the steel [4, 6]. Correspondingly, there is an excessive amount of V for carbonitrides M(C,N), which is consumed by the formation of $(Cr,V)_2N$ particles and even the Laves phase. It should be noted that, despite the absence of the two-phase separation, the size of particles of the M(C,N) carbonitrides in the low-carbon steel after creep is 20% smaller than that in P92 steel.

However, the two-phase separation of carbonitrides into vanadium-enriched and niobium-enriched particles in the 10Kh9V2MFBR steel is the cause of the lower growth rate of particles. The particle size upon creep increases by a factor of 1.5, while in the low-carbon steel, it increases by a factor of almost 2.5 (Table 1). The V/Nb ratio in the M(C,N) carbonitrides in the 02Kh9V2MFBR steel increases from 1 to 1.6.

It was shown in [18] that no growth of plate-like particles of M(C,N) carbonitrides occurs in the low-carbon steel with cobalt during the creep test for 501 h. Their dissolution occurs only after the onset of the formation of the Z phase [18]. It should be noted that, in this study, no particles of the Z phase Cr(V,Nb)N [7, 28–33] were found in steels studied. This is apparently associated with the fact that the time of creep tests was too short for it to form [34].

RESULTS AND DISCUSSION

The results show that a decrease in the amount of carbon in steel leads to changes in the dislocation structure of martensite, as well as in the nature, distribution, and volume fraction of the particles of second phases. These changes exert differently directed influence on the creep resistance of the steel of the P92 type. The main changes in the structure and phase composition of the steel with a lowered carbon content after

tempering are the appearance of a large amount of δ ferrite and the precipitation of particles of the $(Cr,V)_2N$ nitrides, a significant decrease in the volume fraction of $M_{23}C_6$ carbides, and an increase in their size. However, these changes do not affect the static mechanical properties and hardness.

In this study, we did not reveal a negative influence of the formation of δ ferrite on the creep resistance as was found in steel P122 with 11 wt % Cr in [35]. It seems likely that the precipitation strengthening upon creep is more significant than the softening due to the presence of δ ferrite in the structure. The long-term creep strength of the 02Kh9V2MFBR steel increases in comparison with the P122 steel.

In addition to the influence on the second phases, a decrease in the carbon content lowers the solubility of elements such as W and Mo in the solid solution, which provide a solid-solution strengthening and, most importantly, decrease the diffusion rate, which suppresses the recovery processes [1, 2]. This effect is not observed in steels with 3 wt % Co [6, 12, 14, 15, 18–21], since Co increases the solubility of these elements in the ferrite matrix. The escape of W and Mo from the solid solution with the formation of a large amount of the Laves phase facilitates dislocation climb. It seems likely that the development of recovery processes leads to a dramatic decrease in the dislocation density, which is the cause of creep acceleration after 10^3 h of creep tests (Fig. 5). These facts indicate the key role of carbonitrides in the creep strength of martensitic steels with 9 wt % Cr. However, the alloying of the solid solution with W and Mo also substantially affects the creep resistance of the high-chromium martensitic steels.

CONCLUSIONS

(1) A decrease in the carbon content in the 10Kh9V2MFBR steel from 0.1 to 0.018 wt % leads to the formation of δ ferrite with a volume fraction of up to 23%.

(2) The main contribution to the precipitation hardening in the 02Kh9V2MFBR steel comes from particles of the $(Cr,V)_2N$ nitride, which are uniformly distributed in the structure and have an average size of 72 nm and *MX* carbontrides, which have an average size of 15 nm after tempering. The volume fraction of particles of the $M_{23}C_6$ carbides decreased by more than threefold, and their average size after tempering is five times larger that in the 10Kh9V2MFBR steel.

(3) The variations in the phase composition of the 02Kh9V2MFBR steel compared to the 10Kh9V2MFBR steel had no effect on the hardness, yield stress, and ultimate strength at room temperature and at elevated temperatures. The time to fracture of the 02Kh9V2MFBR steel is longer by a factor of two to three after the short-term (up to 1000 h) creep tests. No distinctions in the long-term creep strength of steels was found in the case of the creep test duration of longer than 1000 h.

(4) Uniformly distributed nitrides and carbonitrides efficiently suppress the growth of laths upon creep. The lath/subgrain size is the same in both studied steels after creep at 650°C under the applied stress of 118 MPa.

(5) The amount of the Laves phase precipitated in the 02Kh9V2MFBR steel upon creep is two times larger than that in the 10Kh9V2MFBR steel. This leads to a decrease in the solid-solution strengthening and to a more substantial decrease in the dislocation density in the 02Kh9V2MFBR steel upon creep.

AKCNOWLEDGMENTS

This study was supported in part by the Russian Scientific Foundation, project no. 14-29-00173.

We thank the Center of Collaborative Access "Diagnostics of the Structure and Properties of Nanomaterials" at the Belgorod State National Research University for the equipment supplied for structural investigations.

REFERENCES

1. *Creep-Resistant Steels*, Ef. by F. Abe, T.-U. Kern, and R. Viswanathan (Woodhead, Cambridge, 2008).
2. R. O. Kaybyshev, V. N. Skorobogatykh, and I. A. Shchenkova, "New martensitic steels for thermal power plant: Creep resistance," Phys. Met. Metallogr. **109**, 186–200 (2010).
3. A. Kostka, K. Tak, R. J. Hellmig, Y. Estrin, and G. Eggeler, "On the contribution of carbides and ultra-fine boundaries to the creep strength of tempered martensitic ferritic steels," Acta Mater. **55**, 539–550 (2007).
4. N. Dudova, A. Plotnikova, D. Molodov, A. Belyakov, and R. Kaibyshev, "Structural changes of tempered martensitic 9% Cr–2% W–3% Co steel during creep at 650°C," Mater. Sci. Eng., A **534**, 632–639 (2012).
5. V. Dudko, A. Belyakov, D. Molodov, and R. Kaibyshev, "Microstructure evolution and pinning of boundaries by precipitates in a 9 pct. Cr heat resistant steel during creep," Metall. Mater. Trans. A **44**, 162–172 (2013).
6. I. Fedorova, A. Belyakov, P. Kozlov, V. Skorobogatykh, I. Shenkova, and R. Kaibyshev, "Laves-phase precipitates in a low-carbon 9% Cr martensitic steel during aging and creep at 923 K," Mater. Sci. Eng., A **615**, 153–163 (2014).
7. R. Agamennone, W. Blum, C. Gupta, and J. K. Chakravartty, "Evolution of microstructure and deformation resistance in creep of tempered martensitic 9–12% Cr–2% W–5% Co steels," Acta Mater. **54**, 3003–3014 (2006).
8. G. H. Armaki, R. Chen, K. Maruyama, and M. Igarashi, "Creep behavior and degradation of subgrain structures pinned by nanoscale precipitates in strength-enhanced 5 to 12 Pct Cr ferritic steels," Metall. Mater. Trans. A **42**, 3084–3094 (2011).

9. F. Abe, "Analysis of creep rates of tempered martensitic 9% Cr steel based on microstructure evolution," Mater. Sci. Eng., A **510–511**, 64–69 (2009).
10. K. Suzuki, S. Kumai, Y. Toda, H. Kushima, and K. Kimura, "Two-phase separation of primary *MX* carbonitride during tempering in creep resistant 9Cr1MoVNb steel," ISIJ Int. **43**, 1089–1094 (2003).
11. A. Yu. Kipelova, A. N. Belyakov, V. N. Skorobogatykh, I. A. Shchenkova, and R. O. Kaibyshev, "Tempering-induced structural changes in steel 10Kh9K3V1M1FBR and their effect on mechanical properties," Met. Sci. Heat. Treat. **52**, 100–110 (2010).
12. M. Taneike, K. Sawada, and F. Abe, "Effect of carbon concentration on precipitation behavior of $M_{23}C_6$ carbides and *MX* carbonitrides in martensitic 9Cr steel during heat treatment," Metall. Mater. Trans. A **35**, 1255–1262 (2004).
13. F. J. Humphreys and M. Hatherly, *Recrystallization and Related Annealing Phenomena*, 2nd ed. (Elsevier, Atlanta, GA, 2004),
14. M. Taneike, F. Abe, and K. Sawada, "Creep-strengthening of steel at high temperatures using nano-sized carbonitride dispersions," Nature **424**, 294–296 (2007).
15. F. Abe, M. Taneike, and K. Sawada, "Alloy design of creep resistant 9Cr steel using a dispersion of nano-sized carbonitrides," Int. J. Press. Vess. Pip. **84**, 3–12 (2007).
16. I. I. Gorbachev, V. V. Popov, and A. Yu. Pasynkov, "Thermodynamic modeling of carbonitride formation in steels with V and Ti," Phys. Met. Metallogr. **113**, 974–981 (2012).
17. I. I. Gorbachev, V. V. Popov, and A. Yu. Pasynkov, "Simulation of evolution of precipitates of two carbonitride phases in Nb- and Ti-containing steels during isothermal annealing," Phys. Met. Metallogr. **114**, 741–751 (2013).
18. I. Fedorova, A. Kipelova, A. Belyakov, and R. Kaibyshev, "Microstructure evolution in an advanced 9 Pct Cr martensitic steel during creep at 923 K (650°C)," Metall. Mater. Trans. A **44**, 128–135 (2013).
19. F.-S. Yin and W.-S. Jung, "Nanosized *MX* precipitates in ultra-low-carbon ferritic/martensitic heat-resistant steels," Metall. Mater. Trans. A **40**, 302–309 (2009).
20. F.-S. Yin, L.-Q. Tian, B. Xue, X.-B. Jiang, and L. Zhou, "Effect of carbon content on microstructure and mechanical properties of 9 to 12 Pct Cr ferritic/martensitic heat-resistant steels," Metall. Mater. Trans. A **43**, 2203–2209 (2012).
21. L. Helis, Y. Toda, T. Hara, H. Miyazaki, and F. Abe, "Effect of cobalt on the microstructure of tempered martensitic 9Cr steel for ultra-supercritical power plants," Mater. Sci. Eng., A **510–511**, 88–94 (2009).
22. A. Kipelova, M. Odnobokova, A. Belyakov, and R. Kaibyshev, "Effect of Co on creep behavior of a P911 steel," Metall. Mater. Trans. A **44**, 577–583 (2013).
23. Sh. Wang, L. Chang, D. Lin, X. Chen, and X. Huih, "High temperature strengthening in 12Cr–W–Mo steels by controlling the formation of delta ferrite," Metall. Mater. Trans. A **45**, 4371–4385 (2014).
24. W. Yan, P. Hu, L. Deng, W. Wang, W. Sha, Y. Shan, and K. Yang, "Effect of carbon reduction on the toughness of 9CrWVTaN steels," Metall. Mater. Trans. A **43**, 1921–1933 (2012).
25. S. A. Saltykov, *Stereometric Metallography* (Metallurgiya, Moscow, 1976) [in Russian].
26. H. Kitahara, R. Ueji, N. Tsuji, and Y. Minamino, "Crystallographic features of lath martensite in low-carbon steel," Acta Mater. **54**, 1279–1288 (2006).
27. D. Richardot, J.-C. Vaillant, A. Arbab, and W. Bendick, *The T92/P92 book* (Vallourec and Mannesmann Tubes, Boulogne, 2000).
28. R. O. Kaibyshev, V. N. Skorobogatykh, and I. A. Shchenkova, "Formation of *Z*-phase and prospects of application of martensitic steels with 11% Cr for operation above 590°C," Met. Sci. Heat. Treat. **52**, 90–99 (2010).
29. K. Sawada, H. Kushima, M. Tabuchi, and K. Kimura, "Microstructural degradation of Gr.91 steel during creep under low stress," Mater. Sci. Eng., A **528**, 5511–5518 (2011).
30. K. Kimura, K. Sawada, H. Kushima, and K. Kuba, "Effect of stress on creep deformation of ASME grade P92/T92 steels," Int. J. Mater. Res. **99**, 395–401 (2008).
31. N. Dudova, A. Belyakov, T. Sakai, and R. Kaibyshev, "Dynamic recrystallization mechanisms operating in a Ni–20% Cr alloy under hot-to-warm working," Acta Mater. **58**, 3624–3632 (2010).
32. L. Cipolla, H. K. Danielsen, D. Venditti, P. E. Di. Nunzio, J. Hald, and M. A. J. Somers, "Conversion of *MX* nitrides to *Z*-phase in a martensitic 12% Cr steel," Acta Mater. **58**, 669–679 (2010).
33. H. K. Danielsen, P. E. Di. Nunzio, and J. Hald, "Kinetics of *Z*-phase precipitation in 9 to 12 pct Cr steels," Metall. Mater. Trans. A **44**, 2445–2452 (2013).
34. A. E. Fedoseeva, P. A. Kozlov, V. A. Dudko, V. N. Skorobogatykh, I. A. Shchenkova, and R. O. Kaibyshev, Microstructural changes in 10Kh9V2MFBR steel at creep during 40000 hours at 600°C," Phys. Met. Metallogr. (in press).
35. M. Yoshizawa and M. Igarashi, "Long-term creep deformation characteristics of advanced ferritic steels for USC power plants," Int. J. Press. Vess. Pip. **84**, 37–43 (2007).

Translated by N. Korovin